Microchimica Acta (2022) 189: 55
https://doi.org/10.1007/s00604-021-05144-x

ORIGINAL PAPER

Long-wavelength emission carbon dots as self-ratiometric fluorescent nanoprobe for sensitive determination of Zn^{2+}

Yanling Lv[1] · Peihua Li[1] · Chao Liu[1] · Lian Xia[1] · Fengli Qu[1] · Rong-Mei Kong[1] · Zhi-Ling Song[2]

Received: 8 October 2021 / Accepted: 10 December 2021 / Published online: 10 January 2022

Abstract

A novel ratiometric fluorescence nanoprobe based on long-wavelength emission carbon dots (CDs) was designed for high sensitive and selective detection of Zn^{2+}. The CDs were conveniently prepared by a one-step solvothermal treatment of formamide and glutathione (GSH). Under single excitation wavelength (420 nm), the obtained CDs exhibit three emission peaks at 470, 650, and 685 nm, respectively. For the long-wavelength emission region of the CDs, the fluorescence at 685 nm can be quenched with different levels upon the addition of most metal ions. However, the presence of Zn^{2+} not only results in the fluorescence quenching at 685 nm effectively but also enhances at 650 nm remarkably, which may be due to the formation of CD-Zn^{2+} chelate complex inducing the dispersion of CDs aggregates and changes in the group distribution on the surface of CDs. Taking the advantage of the unique fluorescence response induced by Zn^{2+}, the prepared CDs were successfully employed as nanoprobe for self-ratiometric fluorescence determination of Zn^{2+} with F_{650}/F_{685} as signal output. A good linear relationship in the concentration range 0.01 to 2 μM, and a detection limit as low as 5.1 nM has been obtained. The ratiometric nanoprobe was successfully applied to Zn^{2+} determination in human serum samples.

Keywords Fluorescence · Carbon dots · Self-ratiometric nanoprobe · Zn^{2+} determination

Introduction

Zinc, as an indispensable trace element in human life activity, is the second largest trace element in the human body after iron [1–3]. It participates in many physiological and biochemical functions of living cells; thus, it has a vital effect on human life and health such as cell metabolism, gene regulation, and neurotransmission [4–6]. Studies show that the abnormal level of zinc ions (Zn^{2+}) is closely related to many serious neurological diseases, such as Alzheimer's disease, amyotrophic lateral sclerosis, Parkinson's disease, hypoxic ischemia, and epilepsy [7, 8]. Therefore, it is of great importance to detect the Zn^{2+} level precisely in both healthy monitoring and environmental protection fields. Generally, the traditional methods towards Zn^{2+}, including atomic absorption spectrometry (AAS), atomic emission spectrometry (AES), inductively coupled plasma-mass spectrometry (ICP-MS), and high performance liquid chromatography (HPLC), are mature, accurate, and reliable. However, with the improvement of detection requirements, it is still necessary to develop reliable new methods to achieve highly sensitive and selective detection of Zn^{2+}. In recent decades, fluorescence detection technology has become a research hotspot because of its distinct merits such as simple operation, high sensitivity, and selectivity, and real-time monitoring, thus widely used in analytical field now [9]. With respect to the qualitative and quantitative determination of targets, the use of emission intensity at single wavelength usually encounters the problems of insufficient sensitivity and selectivity. This is mainly due to the unavoidable interference arises from the target-independent factors, such as

Yanling Lv and Peihua Li contributed equally to this work.

✉ Rong-Mei Kong
kongrongmei@126.com

✉ Zhi-Ling Song
zhilingsong@qust.edu.cn

[1] School of Chemistry and Chemical Engineering, Qufu Normal University, Qufu, Shandong 273165, People's Republic of China

[2] Key Laboratory of Optic-Electric Sensing and Analytical Chemistry for Life Science, MOE, Shandong Key Laboratory of Biochemical Analysis, College of Chemistry and Molecular Engineering, Qingdao University of Science and Technology, Qingdao , Shandong 266042, People's Republic of China

light scattering by the sample matrix and excitation source fluctuation [10, 11].

In order to conquer these limitations, another ratiometric fluorescence spectral peak can be introduced to design dual-emission ratiometric detection schemes, which have been proven to achieve more reliable determination of specific targets [10–12]. Because the measured ratiometric fluorescence signal output is almost uninterfered by the fluctuation of the light source intensity, the instrument inherent sensitivity, and the matrix background, much more reliable determination of specific targets can be realized [13–17]. Therefore, ratiometric fluorescence method has attracted more and more attention recently [15–18]. Among the previous reported fluorescent determination methods, a lot of ratiometric probes based on organic fluorescence molecules have been applied to the determination of Zn^{2+}. For instance, Sinha et al. designed a long-wavelength ratio-ratio fluorescent probe based on 1,4-dihydroxyanthraquinone with the emission wavelength red-shifted from 544 to 600 nm after recognition of Zn^{2+} [19]. Shuang et al. synthesized 3-(benzo[*d*]thiazol-2-yl)-5-bromosalicylaldehyde-^{4} *N*-phenyl thiosemicarbazone (BTT) for ratiometric sensing of Zn^{2+} ions with a significant blue shift in the maximum emission of BTT from 570 to 488 nm [20]. Lv et al. reported a novel ratiometric-type fluorescent chemosensor (SP), which appending a 3-picolyl thiourea pendant to a porphyrin fluorophore, and applied for Zn^{2+} monitoring in aqueous buffer and in biological samples [21]. Pramod Kumar Mehta et al. synthesized a fluorescent probe based on the symmetric peptide receptor bearing two imidazole and two sulfonamide groups for the ratiometric detection of Zn^{2+} in aqueous solution [22]. However, in condition to the needs of high sensitivity and selectivity, low toxicity, good water solubility, and stability should also be considered for the development of fluorescence probes for the application of biological and environmental samples. Therefore, it is strongly necessary to develop novel approach for the detection of Zn^{2+} to conquer these disadvantages.

As a new type of carbon nanomaterial, carbon dots (CDs) exhibit fascinating photoluminescence properties such as strong light stability and resistance to photobleaching, adjustable emission wavelength, and longer fluorescence lifetime, which is considered as an excellent electron donor [23, 24]. In addition, many CDs usually have large Stokes shifts, which can avoid the overlap of the emission spectrum and the excitation spectrum, which is conducive to the detection of fluorescence spectral signals [25]. Compare to the fluorescent nanomaterials that composed of other elements, CDs have low toxicity and good biocompatibility. For example, CDs can enter the interior of the cell through endocytosis without affecting the nucleus [26]. Therefore, CDs are attracting considerable attention in the fields of biosensing, bioimaging, biomedicine, and optoelectronic materials in recent years [26, 27]. In addition, compare with the organic fluorescence molecules and other fluorescence nanomaterial-based probes, another important feature of CDs is that they can be synthesized by simple and facile methods. Therefore, synthesis and employ CDs as the fluorescence nanoprobes for the determination of Zn^{2+} are attracting more and more attention in recent years [28]. Despite many of these CDs-based nanoprobes exhibited basic satisfactory analytical performance towards Zn^{2+}, several unsolved issues may be limited their further practical applications. For example, some CDs-based nanoprobes needed the introduction of organic molecules or other nanomaterials as recognition/signal-out moiety by covalently linking, which brings with the problems such as complexity of probe construction, toxicity, and increased cost. Moreover, most of the nanoprobes based on the single-signal output mode, which usually led to poor selectivity, susceptible to influence of light source intensity fluctuation, probe concentration, background fluorescence, and environmental effect. In addition, fluorescent nanoprobes with long-wavelength emission are more suitable for biological samples, since they could reduce the autofluorescence interference of the sample matrix. Therefore, under the great incentive of the above problems, it is highly urgent to do more promoting work on long-wavelength emitted CDs-based self-ratiometric fluorescent probes towards Zn^{2+}, which can not only be simple and facile synthesized but also with improving analytical performance.

In this study, a novel multi-emission CDs was conveniently prepared by a one-step solvothermal treatment of formamide and glutathione (GSH). Under a single excitation at 420 nm, the obtained CDs exhibit three emission peaks at 470, 650, and 685 nm, respectively. We found that the presence of Zn^{2+} could lead to a specific ratiometric fluorescence response in the long-wavelength emission region of the CDs (Scheme 1). Specifically, the fluorescence at 685 nm was effectively quenched upon the addition of Zn^{2+}, while the fluorescence at 650 nm was enhanced remarkably. Therefore, the unique fluorescence response induced by Zn^{2+} endows with CDs the ability to be used as self-ratiometric fluorescence nanoprobe for the determination of Zn^{2+}. Taking the fluorescence intensity ratio at 650 and 685 nm (F_{650}/F_{685}) as the signal output, improving sensitivity and selectivity towards Zn^{2+} was obtained.

Experimental section

Preparation of the CDs

The preparation of CDs refers to the reported procedure with modification [29]. The synthesis process is described in detail in the electronic supplementary material.

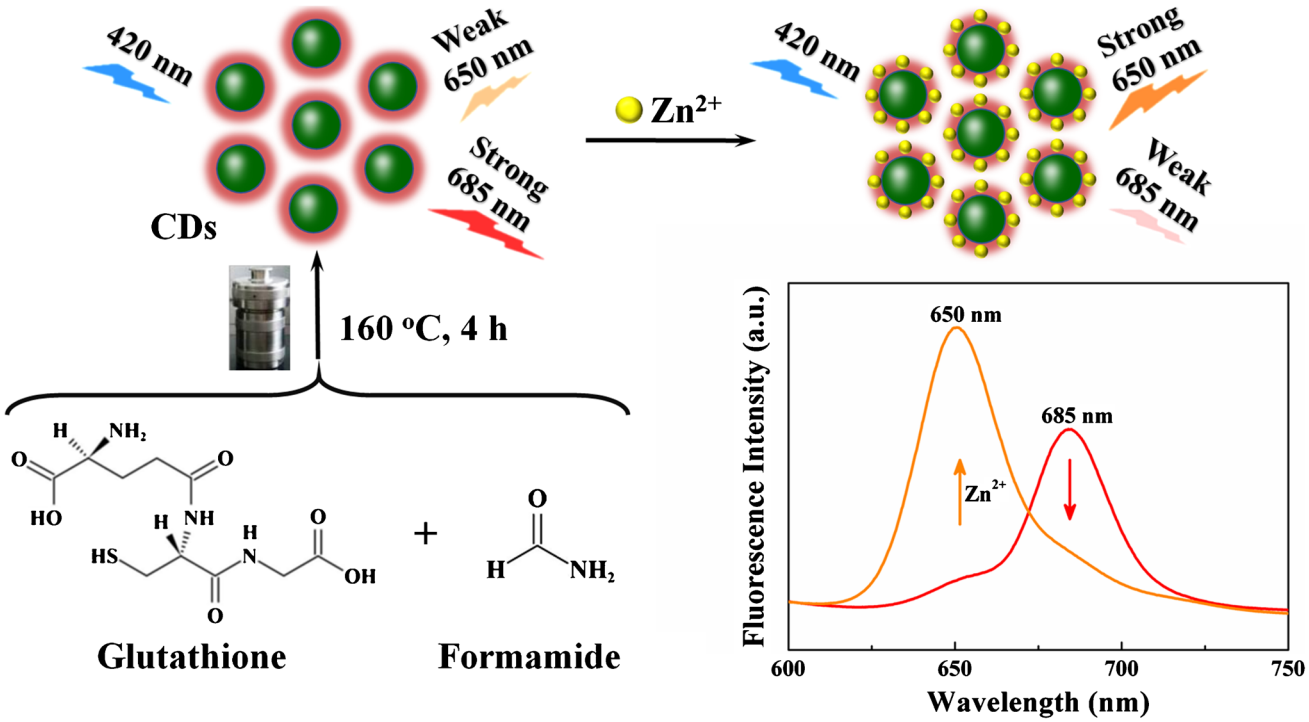

Scheme 1 Schematic illustration of the preparation of CDs and the application as ratiometric fluorescence nanoprobe for the detection of Zn^{2+}

Determination of Zn^{2+}

Using the prepared CDs as the ratiometric fluorescence probe for Zn^{2+} determination was performed as the following procedure: adding 100 μL of the Zn^{2+} solution with different concentrations into 400 μL of CDs solution (100 times diluted with PBS buffer) and then mixed thoroughly and allowed to react at room temperature for 25 min. After that, the fluorescence emission spectra were measured in the wavelength range from 600 to 750 nm under the excitation at 420 nm. For the selectivity investigation, the fluorescence responses of the CDs nanoprobe to some common metal ions were measured under the same conditions. For the real sample application investigation, the experiments were conducted in diluted human serum samples. Specifically, the human serum sample was diluted 100 times with PBS buffer and then tested according to Zn^{2+} determination procedure. The recovery tests were performed by spiking a certain amount of Zn^{2+} standard solution (0.2, 0.5, 1.0 μM) into the diluted human serum samples. Atomic absorption spectroscopy (AAS) was used as the reference method to demonstrate the developed method. Informed consent was obtained from human participants of this study. The serum sample experiments were approved by the Ethical Committee of Qufu Normal University and performed according to its Guidelines.

Results and discussion

Characterization of the synthesized CDs

Considering the possessing of special physical and chemical properties, such as good dissolving capacity and metal reaction adduct ability, formamide was selected as one of the raw materials and solvent for the synthesis of CDs. Meanwhile, GSH was selected as the other one raw material for the synthesis of CDs due to the containing of C, N, and S elements. Briefly, the CDs were prepared facilely through solvothermal treatment of a solution of GSH in formamide at 160 °C for 4 h (Scheme 1). After the reaction, the final dark-green solution represents the formation of CDs. The TEM characterization was performed to study the morphology and size of the prepared CDs. As can be seen from Fig. 1A, most of the CDs exist in aggregates with the aggregation size of about 25–35 nm. The high-resolution TEM (HRTEM) shows that the CD particles in aggregates are quasi-spherical in shape and have clear lattice fringes (Fig. 1B), indicating their crystalline nature with graphitic core [30]. The CD particle size distribution is ranging in 3–5 nm with an average particle size of approximately 4.0 nm. This aggregation phenomenon may be due to the covering of various groups containing H, N, and O elements on CDs surface resulted the formation

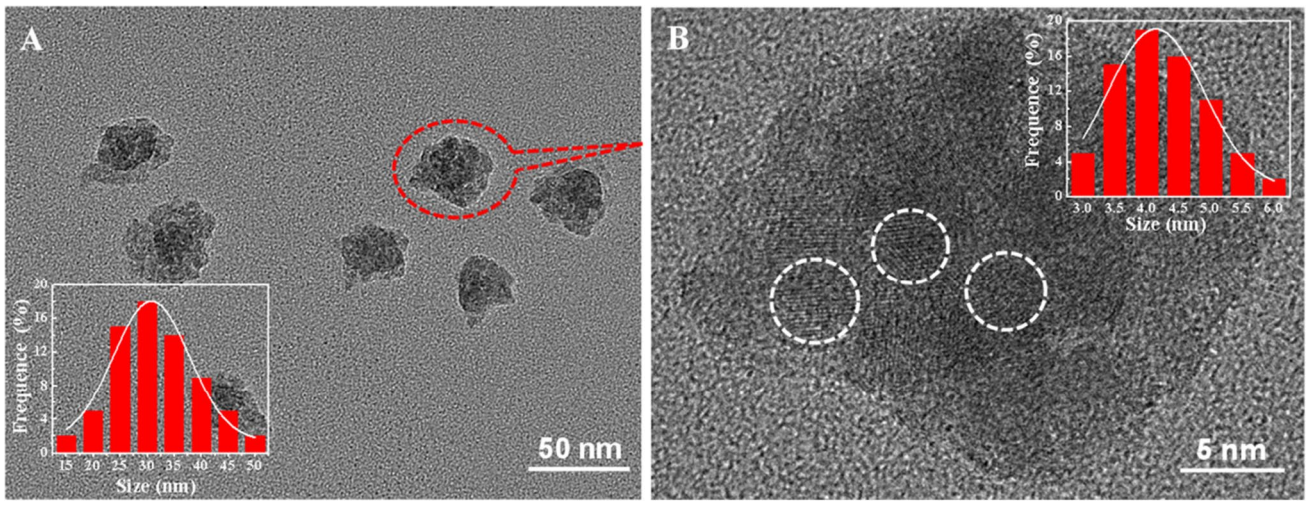

Fig. 1 **A** TEM image of the CDs in aggregated state. Inset: the size distribution histogram of CDs aggregations. **B** HRTEM image of the CDs in aggregated state. Inset: the size distribution histogram of CDs particles

of hydrogen bonding forces between CD particles. In addition, the dilution experimental result indicated that under the condition of gradual dilution with PBS buffer, the aggregation phenomenon of CDs will decrease and even disperse completely (Fig. S1). This may be because the hydrogen bonding forces between the hydrophilic groups on the surface of CDs and water molecules gradually increases, leading to the improvement of their dispersion. In addition, the experiment result indicated that the prepared CDs are not only easily dispersed as small aggregates with uniform size in PBS buffer but also with high stability that can be maintained in solution state for a month without sedimentation. This excellent property may be attributed to the various water-soluble groups on the surface of CDs, such as carboxyl (-COOH), hydroxyl (-OH), amino (-NH_2), and amide (-$CONH_2$), which were derived from the raw materials of formamide and GSH for CDs. Figure 2A shows the XRD profile of the prepared CDs, a broad peak at $2\theta = 23.88°$ can be observed which corresponds to the (002) plane of graphite, indicating the presence of graphitic carbon domain in the prepared CDs [29]. The XRD result is in consistent with the result characterized by HRTEM.

The surface element compositions and states of the prepared CDs were measured by XPS. As shown in Fig. 2B, the characteristic peaks of CDs can be obviously observed, including four peaks at 285, 400, 532, and 163 eV corresponding to C 1 s, N 1 s, O 1 s, and S 2p, respectively, indicating the existence of C, N, O, and S elements [12, 29]. Therefore, the surface of the CDs may be passivated with N, O, and S containing functional groups, which may be beneficial to the possibility of achieving long wavelength emission. The high-resolution spectrum of C 1 s shows the presence of C–C/C = C (284.7 eV), C-S (285.4 eV), and N–C = O (289.1 eV) bonds, respectively (Fig. S2A). The high-resolution spectrum of N 1 s is fitted with three binding energies at 396.7, 398.7, and 401.1 eV, which are attributed to the C-N–C, pyrrolic-like N, and graphitic N, respectively (Fig. S2B). The four fitting peaks of high-resolution spectrum of S 2p at 161.3, 162.9, 165.0, and

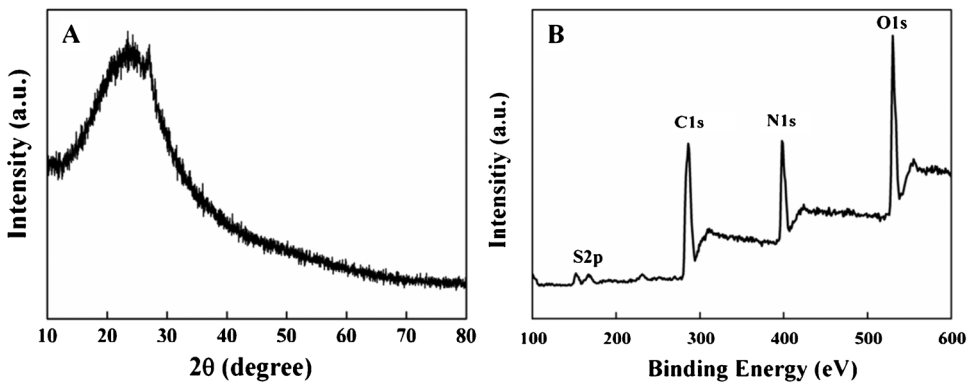

Fig. 2 **A** XRD pattern of the CDs. **B** XPS survey of the CDs

168.8 eV are attributed to thiolate, $2p_{3/2}$ and $2p_{1/2}$ of S, S = O, respectively (Fig. S2C). The high-resolution spectrum of O 1 s is resolved into three binding energies at 528.7, 530.4, and 532.6 eV, which can be assigned to C-O, C = O, C–O–C/C–OH (Fig. S2D).

The FTIR measurement was carried out to clarify the surface group states of the prepared CDs. As shown in Fig. 3, the FTIR spectrum exhibits several absorption maxima/bands. The broad peak at 3408 cm^{-1} is assigned to the O–H and N–H stretching vibrations, proving the presence of -OH and -NH_2. The peak at 1673 cm^{-1} corresponds to the stretching vibration of C = O, whereas the peak at 1115 cm^{-1} is from the stretching vibration of C-O. The peak at 1392 cm^{-1} is attributed to the stretching vibration of C-N and deformation vibration of N–H. The peak at 617 cm^{-1} is attributed to N–H bond. Therefore, the above absorption peaks according to O–H, N–H, C = O, and C-N vibrations indicated the presence of -COOH and -CONH-/-$CONH_2$ which are attached to the aromatic core of the CD particle. Obviously, the FTIR characteristic results are well with those of XPS characterization.

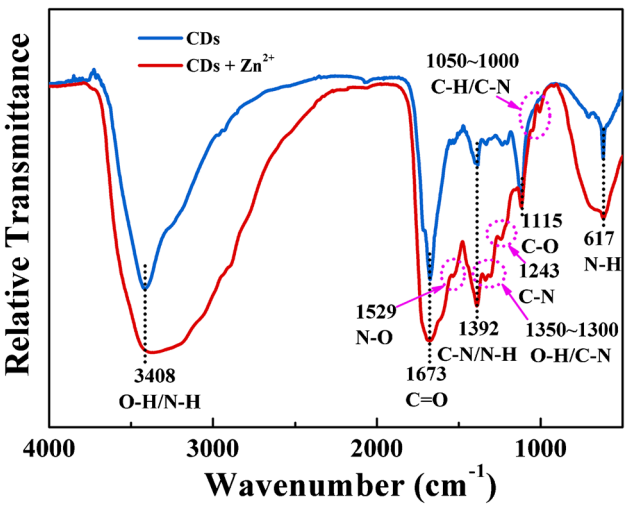

Fig. 3 FTIR spectra of the CDs before and after addition of Zn^{2+}

Optical properties of the synthesized CDs

The optical performance characteristics of CDs were investigated by measuring the UV–Vis absorption spectrum and fluorescence spectra (Fig. 4). As shown in Fig. 4A, the UV–Vis absorption spectrum of CDs exhibits several main absorptions ranging from 300 to 500 nm, which is produced by the electronic transition of aromatic conjugated systems containing C = O, C = N, and C = S bonds of CDs [29]. As there is an absorbance peak at about 420 nm, the fluorescence emission spectra were investigated when excited within the wavelength range of 400–440 nm. As shown in Fig. S3, one short wavelength emission peak within the range of 450–510 nm and two emission peaks at 650 and 685 nm, respectively, can be observed. The emission maxima of the short wavelength emission gradually red shift, whereas the emission intensity gradually decreased with the increase of the excitation wavelength. Meanwhile, the long wavelength emission intensity at 685 nm gradually decreased while at 650 nm increased first then decreased. As the TEM, XPS, and FTIR characterization of CDs above, the possible functional groups, adsorbed molecules, impurities, and surface defects of CDs can result in the trap states in the bandgap, which may be responsible for the above emission phenomenon [30]. In this case, the photoexcited electron and/or hole can be trapped, and their following recombination leads to a lower energy and higher wavelength radiative emission. The fluorescence emission spectra of CDs in Fig. 4B shows three emission peaks at 470 nm, 650 nm, and 685 nm, respectively, under the excitation wavelength of 420 nm. Fixed the emission wavelengths at 650 nm and 685 nm, respectively, the corresponding maximum excitation wavelengths obtained are 421 nm and 417 nm, respectively. Considering the advantages of long wavelength emission with large Stokes shift in biosensing, it is necessary to obtain the emission intensities at 650 nm and 685 nm as high as possible, thus selecting 420 nm as the excitation wavelength for subsequent experiments.

Fig. 4 **A** UV–Vis absorption spectrum and **B** fluorescence emission and excitation spectra of the CDs

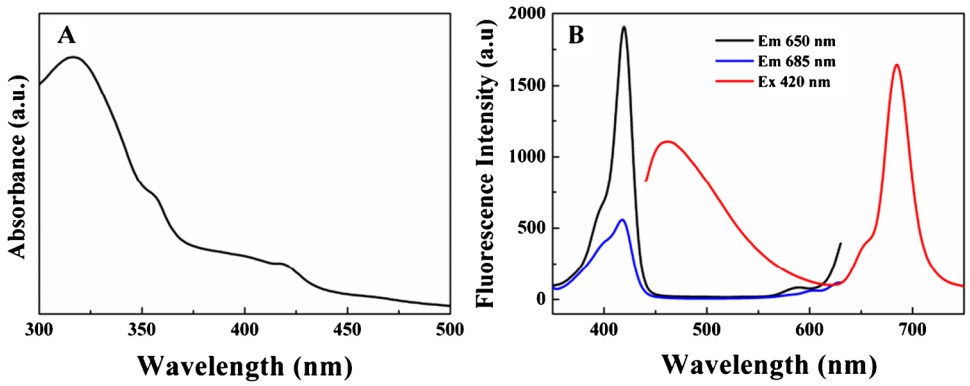

Speculation on principle of ratiometric fluorescence detection of Zn^{2+}

The zeta potential measurement (− 11.2 mV) indicates that the CDs surface are negatively charged due to the easy donate proton ability of predominantly covered -COOH and -OH groups (Fig. S4). Therefore, the positively charged Zn^{2+} can be adsorbed on the CDs surface by electrostatic interaction with the zeta potential positively change. In addition, the groups such as -NH_2 and -CONH-/-$CONH_2$ are also covered on the CDs surface, indicating the possibility to bind Zn^{2+} through chelation. The electrostatic interaction and chelation may be resulted in the distribution change of the surface groups on CDs. Therefore, the addition of Zn^{2+} into CDs system may disrupt the aggregation state of the CDs. This can be evidenced by TEM characterization. As shown in Fig. S5, the TEM image of Zn^{2+}-CDs system shows that the presence of Zn^{2+} resulted in good dispersion of CDs as single CD particle. As expected, the particle size and lattice fringes have no changes as compared with the CDs particles in the aggregates (Fig. 1). The FTIR spectrum of Zn^{2+}-CDs system was further tested to investigate the above speculation. As shown in Fig. 3, the presence of Zn^{2+} results in a larger absorption peak of the main groups on CDs surface, but has no obvious effect on the peak frequency. This is because the good dispersion of CDs caused by Zn^{2+} endows CD particles with better exposure of the surface groups. The appearance of peaks at 1000–1050 cm^{-1}, 1243 cm^{-1}, and 1350–1300 cm^{-1} referred to C-H/C-N, C-N, and O–H/C-N bonds, respectively, also evidenced the better exposure of the CDs surface groups. The wide peak within the range of 3000 cm^{-1} to 3600 cm^{-1} has no peak shifting, indicating the electrostatic interaction between -OH/-COOH and Zn^{2+}. The new peak appeared at 1040 cm^{-1} is generally referred to the C-N stretching vibration of aliphatic amine, which can coordinate with Zn^{2+}. Another evidence is the appearance of new peak at 1526 cm^{-1} corresponds to N–O bond, which may be due to the conversion of N = O bond resulted from the coordination complex.

Then, the fluorescence responses of CDs after the incubation with Zn^{2+} were investigated. Interestingly, as shown in Fig. 5, the addition of Zn^{2+} into the CDs sensing system can specifically induce the decrease of the fluorescence at 685 nm, together with the significant increase of fluorescence at 650 nm. Therefore, a significant increase of the ratio value of F_{650}/F_{685} (the F_{650} and F_{685} refer to the fluorescence intensity at 650 nm and 685 nm, respectively) can be resulted. Taking the ratio value of F_{650}/F_{685} as signal output, the CDs can be potentially employed as ratiometric fluorescence nanoprobe for Zn^{2+} determination. In addition, the presence of Zn^{2+} induces the increase of the excitation intensity at 421 nm for the 650 nm emission while decreases at 417 nm for the 685 nm. As can be seen from Fig. 6A, the

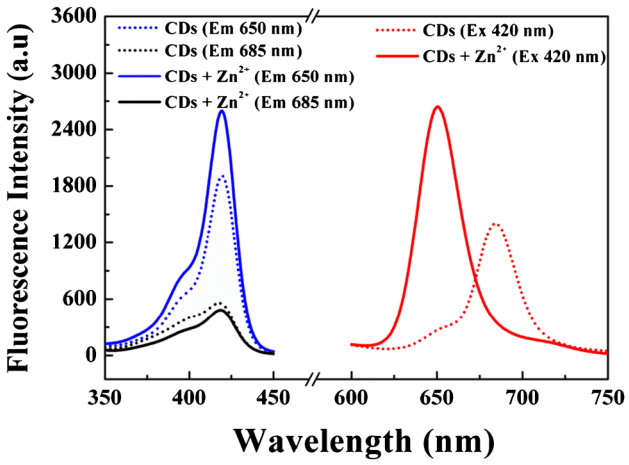

Fig. 5 The fluorescence excitation (left) and emission (right) spectra of the CDs before and after addition of Zn^{2+}

UV–Vis absorption spectrum of CDs in the presence of Zn^{2+} shows an obvious increase of absorption at 421 nm compare to that of CDs only, which consist well with the fluorescence excitation and emission spectra.

Specifically, the static quenching and dynamic quenching can be distinguished by measuring the fluorescence lifetime of CDs before and after incubation with quenchers. If the value has almost no change, static quenching is responsible for the quenching process. If obviously becomes shorter, it is dynamic quenching [31]. The fluorescence decay curves of CDs before and after binding of Zn^{2+} are shown in Fig. 6B; slightly change of the average fluorescence lifetime can be observed, indicating that the fluorescence quenching at 685 nm is caused by the static quenching. Moreover, the fluorescence lifetime test result further confirmed the formation of CDs-Zn^{2+} complex.

Optimization of experimental conditions

In order to obtain the optimal analytical conditions, the effects of the pH and CDs concentration on the CDs fluorescence and Zn^{2+} incubation time on the analytical performance of the sensing system were investigated. Due to the different surface groups of CDs prepared by different methods, the fluorescent responses to pH are usually complicated. Therefore, the effect of pH on the CDs fluorescence was explored firstly. Figure S6A shows the fluorescence responses of CDs in various pH environments (pH 5.0 to pH 9.0). The dual emission intensities of CDs remain almost unchanged in the pH range from 5.0 to 7.5, whereas exhibit the obvious decrease at 685 nm and increase at 650 nm with the further rise of pH value from 8.0 to 9.0, which is assumed to the deprotonation of surface groups of CDs along with the rise of pH value and tautomerism between the structures of -NH-C = O and -N = C–OH on CDs surface. Therefore, in

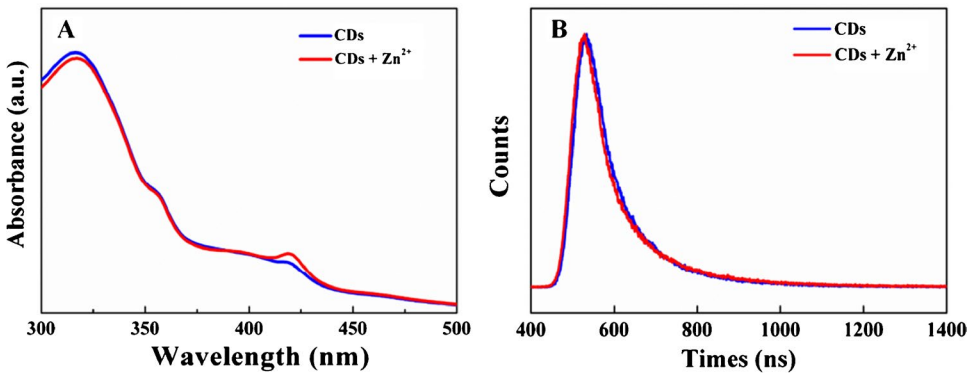

Fig. 6 **A** UV–Vis absorption spectra and **B** PL decays of CDs at 685 nm before and after addition of Zn^{2+}

order to maintain the fluorescence stability of the CDs, the PBS buffer solutions with pH 7.0 were utilized for the following experiments. The fluorescence probe concentration also plays an important role in the entire experimental process. Then, the relationship between the CDs dilution multiple and the fluorescence emission intensity was investigated. As depicted in Fig. S6B, the emission at 685 nm increases first and then decreases with the increase of CDs dilution ratio in the range of 10 to 600 times, thus selecting of 100 diluted times as the optimal CDs concentration. Finally, the Zn^{2+} incubation time was investigated. Figure S6C show that the value of F_{650}/F_{685} increases with the increase of incubation time and nearly unchanged after 15 min. Considering the requirement of complete reaction between CDs and Zn^{2+} for the quantitative analysis, 20 min is chosen as the optimal reaction time in the following experiments.

Performance of ratiometric fluorescence determination of Zn^{2+}

In order to further confirm the feasibility of this CDs-based nanoprobe for ratiometric fluorescence determination of Zn^{2+} with specificity, we investigated the fluorescence responses of other 18 common metal ions. As shown in Fig. 7, after the addition of other metal ions including Na^+, K^+, Ag^+, Hg^{2+}, Pb^{2+}, Cd^{2+}, Ca^{2+}, Cu^{2+}, Fe^{2+}, Ni^{2+}, Mn^{2+}, Co^{2+}, Mg^{2+}, Fe^{3+}, Al^{3+}, Ce^{3+}, and In^{3+} into the CDs sensing system, almost all of these metal ions exhibit obvious fluorescence quenching at 685 nm while slight effects on the fluorescence at 650 nm of CDs. However, only the presence of Zn^{2+} not only can induce the fluorescence quenching at 685 nm but also increase at 650 nm significantly. The mixtures of Zn^{2+} with interfering metal ions also exhibited satisfactory ratiometric fluorescence responses (Fig. S7). This response phenomenon may be explained to the unfilled D-orbital of some investigated interfering metals ions which can trap the photoexcited electrons of CDs and thus quenching the fluorescence. For Hg^{2+}, as a heavy metal ion with larger size, it can usually coordinate with aromatic amino-like or sulfur-containing groups on CDs surface to cause strong quenching [30]. However, the closed shell D-orbital of Zn^{2+} limits its ability to trap photoexcited electron but synergies with the complexation of CDs-Zn^{2+} to trigger a special ratiometric fluorescence response. Therefore, these

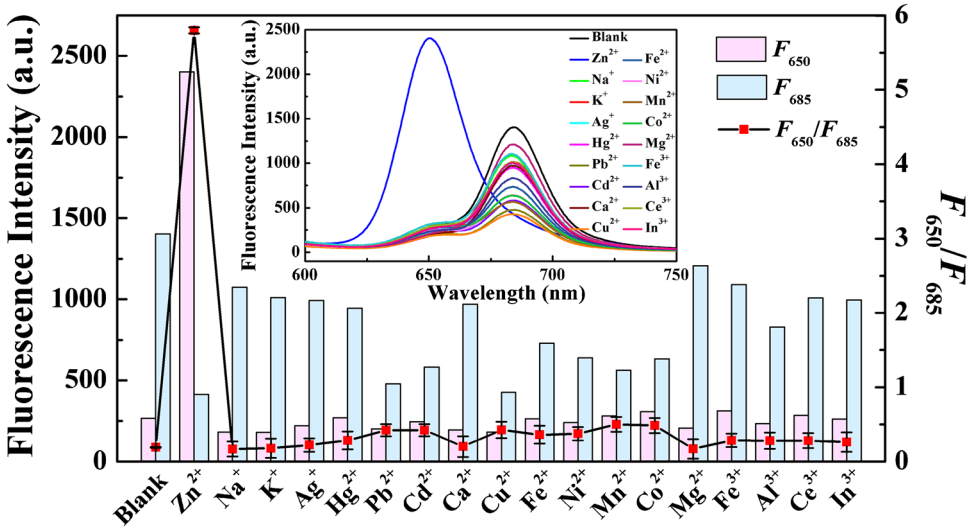

Fig. 7 The responses of CDs to different metal ions. The concentration of each metal ion was 1 μM. Error bars were estimated from three replicate measurements

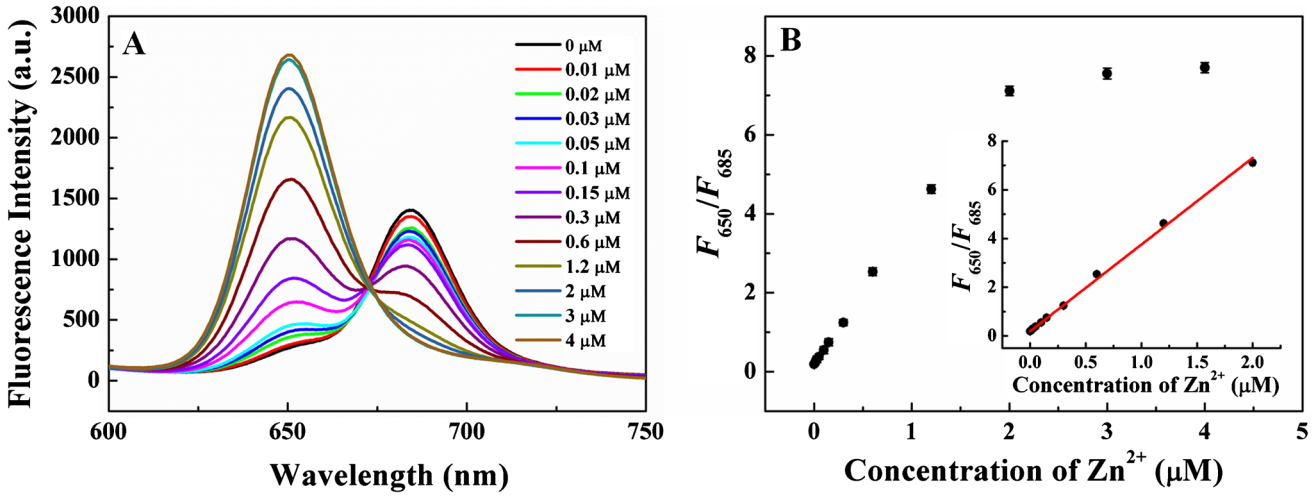

Fig. 8 **A** The fluorescence spectra of the CDs nanoprobe in the presence of different concentrations of Zn^{2+}. **B** The relationship between the concentration of Zn^{2+} and the value of F_{650}/F_{685}. Inset: the linear region at low concentrations of Zn^{2+}. Error bars were estimated from three replicate measurements

results indicated that the prepared CDs are very suitable as ratiometric fluorescence nanoprobe for the selective determination of Zn^{2+}.

Then, the fluorescence response spectra and corresponding F_{650}/F_{685} values of CDs sensing system towards different concentration of Zn^{2+} were investigated under optimized experimental conditions. As shown in Fig. 8A, with the increase of Zn^{2+} concentration ranging from 0 to 4 μM, the fluorescence intensity of CDs gradually increases at 650 nm while decreases at 685 nm. Correspondingly, the ratio value of F_{650}/F_{685} gradually increases with increasing concentration of Zn^{2+} (Fig. 8B). The value of F_{650}/F_{685} shows a good linear relationship with the concentration of Zn^{2+} in the range of 0.01–2 μM. The linear regression equation is $F_{650}/F_{685}=0.191+3.562C_{Zn}2+$ with high correlation coefficient ($R^2=0.998$). Based on the 3σ rule ($\sigma=3S/k$, S is the standard deviation in the blank solution after 10 times repeated measurements, and k is the slope of the standard curve), the detection limit is estimated as low as 5.1 nM. The analytical performance comparison of this proposed CDs-based fluorescence nanoprobe with the previous reports about fluorescent assay for Zn^{2+} was illustrated in Table S1. One can be seen that the proposed CDs-based fluorescence nanoprobe not only offered a superior detection limit for Zn^{2+} but also exhibited excellent selectivity owing to the Zn^{2+}-induced unique ratiometric emission response. Moreover, the long-wavelength emission property and convenient preparation process of the CDs further improve the real sample application possibility.

Determination of Zn^{2+} in human serum samples

To explore the feasibility of the CDs-based ratiometric nanoprobe to be applied for complex biological samples, the recovery assay for Zn^{2+} in diluted human serum samples (1%) was performed. The serum samples with spiked Zn^{2+} of different concentrations (0.2, 0.5, and 1 μM) were measured according to the procedure in buffer system. As shown in Table 1, the acceptable recoveries in the range from 95.0 to 105.0% with relative standard deviation (RSD) less than 5.0% were obtained. In addition, AAS was used as a reference method to demonstrate the developed method. The

Table 1 Recovery test of Zn^{2+} in spiked human serum samples analyzed by the CDs-based ratiometric fluorescence nanoprobe

Sample	Added (μM)	Found (μM)		Recovery (%)	RSD ($n=3$, %)
		CDs	AAS		
Serum I	0.2	0.21 ± 0.01	0.20 ± 0.01	105.0	3.6
	0.5	0.48 ± 0.02	0.49 ± 0.01	96.0	4.9
	1.0	1.03 ± 0.01	1.02 ± 0.01	103.0	3.5
Serum II	0.2	0.19 ± 0.01	0.20 ± 0.02	95.0	4.6
	0.5	0.52 ± 0.02	0.53 ± 0.01	104.0	3.6
	1.0	1.05 ± 0.01	1.05 ± 0.01	105.0	3.7

result indicates that the CDs-based ratiometric fluorescence nanoprobe has great potential to realize the quantitative determination of Zn^{2+} in human serum samples.

Conclusions

A novel multi-emission CDs were prepared by a one-step solvothermal approach, which can be used for the ratiometric fluorescence determination of Zn^{2+}. The presence of Zn^{2+} can specifically enhance the fluorescence at 650 nm remarkably while quench the fluorescence at 685 nm, which may be originated from the change of the surface group distribution of CDs caused by the chelation of Zn^{2+}. Based on the unique ratiometric fluorescence response, the CDs-based nanoprobe successfully realized the high sensitive and selective determination of Zn^{2+}, with a low detection limit of 5.1 nM. Compared with previous reported CD-based nanohybrid ratiometric sensors, the construction of this ratiometric sensor here can be achieved only during CDs preparation process and does not require postmodification with other fluorophores or further mixing. Of course, it is still need to make better use of the short-wavelength emission property of the CDs-based fluorescent nanoprobe and develop better synthesis or purification methods to achieve higher long-wavelength emission quantum yield.

Supplementary Information The online version contains supplementary material available at https://doi.org/10.1007/s00604-021-05144-x.

Funding This work was supported by the Natural Science Foundation of Shandong Province (ZR2020KB020), the National Natural Science Foundation of China (22074080), the Open Project of Chemistry Department of Qingdao University of Science and Technology (QUSTHX201926), and the Graduate Education Innovation Program of Qufu Normal University (CXJ1903).

Declarations

Conflict of interest The authors declare no competing interests.

References

1. Taki M, Wolford JL, O'Halloran TV (2004) Emission ratiometric imaging of intracellular zinc: design of a benzoxazole fluorescent sensor and its application in two-photon microscopy. J Am Chem Soc 126:712–713
2. Choi DW, Koh J-Y (1998) Zinc and brain injury. Annu Rev Neurosci 21:347–375
3. Berg JM, Shi YG (1996) The galvanization of biology: a growing appreciation for the roles of zinc. Science 271:1081–1085
4. Sensi SL, Paoletti P, Bush AI, Sekler I (2009) Zinc in the physiology and pathology of the CNS. Nat Rev Neurosci 10:780–791
5. Franklin RB, Costello LC (2009) The important role of the apoptotic effects of zinc in the development of cancers. J Cell Biochem 106:750–757
6. Maret W (2009) Molecular aspects of human cellular zinc homeostasis: redox control of zinc potentials and zinc signals. Biometals 22:149–157
7. Voegelin A, Pfister S, Scheinost AC, Marcus MA, Kretzschmar R (2005) Changes in zinc speciation in field soil after contamination with zinc oxide. Environ Sci Technol 39:6616–6623
8. Callender E, Rice KC (2000) The urban environmental gradient: ANTHROPOGENIC influences on the spatial and temporal distributions of lead and zinc in sediments. Environ Sci Technol 34:232–238
9. Zhang Z, Wu Y, He S, Xu Y, Li G, Ye B (2018) Ratiometric fluorescence sensing of mercuric ion based on dye-doped lanthanide coordination polymer particles. Anal Chim Acta 1014:85–90
10. Gui R, Jin H, Bu X, Fu Y, Wang Z, Liu Q (2019) Recent advances in dual-emission ratiometric fluorescence probes for chemo/biosensing and bioimaging of biomarkers. Coord Chem Rev 383:82–103
11. Han X, Meng Z, Xia L, Qu F, Kong RM (2020) O-Phenylenediamine/gold nanocluster-based nanoplatform for ratiometric fluorescence detection of alkaline phosphatase activity. Talanta 212:120768
12. Zhao J, Huang M, Zhang L, Zhou M, Chen D, Huang Y, Zhao S (2017) Unique approach to develop carbon dot-based nanohybrid near-infrared ratiometric fluorescent sensor for the detection of mercury ions. Anal Chem 89:8044–8049
13. Huang XL, Song JB, Yung BC, Huang XH, Xiong YH, Chen XY (2018) Ratiometric optical nanoprobes enable accurate molecular detection and imaging. Chem Soc Rev 47:2873–2920
14. Sun W, Han X, Qu F, Kong RM, Zhao Z (2021) A carbon dot doped lanthanide coordination polymer nanocomposite as the ratiometric fluorescent probe for the sensitive detection of alkaline phosphatase activity. Analyst 146:2862–2870
15. Zhao C, Zhang X, Li K, Zhu S, Guo Z, Zhang L, Wang F, Fei Q, Luo S (2015) Forster resonance energy transfer switchable self-assembled micellar nanoprobe: ratiometric fluorescent trapping of endogenous H_2S generation via fluvastatin-stimulated upregulation. J Am Chem Soc 137:8490–8498
16. Han S, Zhang H, Yue X, Wang J, Yang L, Wang B, Song X (2021) A ratiometric, fast-responsive, and single-wavelength excited fluorescent probe for the discrimination of Cys and Hcy. Anal Chem 93:10934–10939
17. Liu R, Zhang L, Chen Y, Huang Z, Huang Y, Zhao S (2018) Design of a New near-infrared ratiometric fluorescent nanoprobe for real-time imaging of superoxide anions and hydroxyl radicals in live cells and in situ tracing of the in flammation process in vivo. Anal Chem 90:4452–4460
18. Liu LY, Zhao Y, Zhang N, Wang KN, Tian M, Pan Q, Lin W (2021) Ratiometric fluorescence imaging for the distribution of nucleic acid content in living cells and human tissue sections. Anal Chem 93:1612–1619
19. Sinha S, Gaur P, Mukherjee T, Mukhopadhyay S, Ghosh S (2015) Exploring 1,4-dihydroxyanthraquinone as long-range emissive ratiometric fluorescent probe for signaling Zn^{2+}/PO_4^{3-}: ensemble utilization for live cell imaging. J Photochem Photobiol B 148:181–187
20. Wu Q, Feng LH, Chao JB, Wang Y, Shuang S (2021) Ratiometric sensing of Zn^{2+} with a new benzothiazole-based fluorescent sensor and living cell imaging. Analyst 146:4348–4356
21. Ying FP, Lu HS, Yi XQ, Xu YQ, Lv YY (2021) A porphyrin platform for ratiometric fluorescence monitoring of Zn^{2+} ion. Sensor Actuat B-Chem 340:129997
22. Mehta PK, Oh ET, Park HJ, Lee KH (2017) Ratiometric fluorescent probe based on symmetric peptidyl receptor with picomolar for Zn^{2+} in aqueous solution. Sensor Actuat B-Chem 245:996–1003

23. Wen Q, Pu Z, Yang Y, Wang J, Wu B, Hu Y, Liu P, Ling J, Cao Q (2020) Hyaluronic acid as a material for the synthesis of fluorescent carbon dots and its application for selective detection of Fe^{3+} ion and folic acid. Microchem J 159:105364
24. Shen R, Song K, Liu H, Li Y, Liu H (2012) Fluorescence enhancement and radiolysis of carbon dots through aqueous gamma radiation chemistry. J Phys Chem C 116:15826–15832
25. Bespalov VG, Kiselev VM, Kislyakov IM, Kozlov SA, Krylov VN, Lukomskii GV, Nesterov LA, Putilin SE, Vysotina NV, Rasanov NN (2009) Anti-stokes self-shift and broadening of the femtosecond laser emission spectrum in a strongly absorbing medium. Opt Spectrosc 106:600–608
26. Baker SN, Baker GA (2011) Luminescent carbon nanodots: emergent nanolights. Angew Chem Int Ed 49:6726–6744
27. Lim SY, Shen W, Gao ZQ (2015) Carbon quantum dots and their applications. Chem Soc Rev 44:362–381
28. Wang B, Liang Z, Tan H, Duan W, Luo M (2020) Red-emission carbon dots-quercetin systems as ratiometric fluorescent nanoprobes towards Zn^{2+} and adenosine triphosphate. Microchim Acta 187:345
29. Pan L, Sun S, Zhang L, Jiang K, Lin H (2016) Near-infrared emissive carbon dots for two-photon fluorescence bioimaging. Nanoscale 8:17350–17356
30. Dastidar DG, Mukherjee P, Ghosh D, Banerjee D (2021) Carbon quantum dots prepared from onion extract as fluorescence turn-on probes for selective estimation of Zn^{2+} in blood plasma. Colloid Surface A 611:125781
31. Yu J, Song N, Zhang YK, Zhong SX, Wang AJ, Chen JR (2015) Green preparation of carbon dots by Jinhua bergamot for sensitive and selective fluorescent detection of Hg^{2+} and Fe^{3+}. Sensor Actuat B-Chem 214:29–35